Protocol and reference material for measuring the nanoantenna enhancement factor in Tip-enhanced Raman Spectroscopy

*

Aroldo Ribeiro Neto
Departamento de Física
Universidade Federal de Minas Gerais
Belo Horizonte, Brazil
aroldoribeiro@ufmg.br

Cassiano Rabelo
Graduate Program in Electrical Eng.
Universidade Federal de Minas Gerais
Belo Horizonte, Brazil
cassianorabelo@ufmg.br

Luiz Gustavo Cançado
Departamento de Física
Universidade Federal de Minas Gerais
Belo Horizonte, Brazil
cancado@fisica.ufmg.br

Michael Engel
IBM Research
Rio de Janeiro, Brazil
mengel@br.ibm.com

Mathias Steiner
IBM Research
Rio de Janeiro, Brazil
mathiast@br.ibm.com

Ado Jorio
Departamento de Física
Universidade Federal de Minas Gerais
Belo Horizonte, Brazil
adojorio@fisica.ufmg.br

***Abstract*—There is up to date no agreement on what is the enhancement factor (f_e) in tip-enhanced Raman Spectroscopy (TERS). The complexity resides both on the lack of a proper theoretical definition and of a reliable experimental procedure for measuring it. Here we propose a protocol and a reference material to characterize the intrinsic f_e value of a TERS nanoantenna. The protocol is based on the theoretical description of the tip-sample approach curve, which should be performed in a reference material made of a well-defined near-field Raman scattering properties together with other specificities that allows measuring all the parameters necessary to fully optimize and characterize the measuring system.**

***Index Terms*—Reference Material, Novel materials and devices, Tip-enhanced Raman Spectroscopy.**

I. Introduction

On tip-enhanced Raman spectroscopy (TERS) [1], the tip, or nanoantenna, must provide a local field enhancement when compared to the Raman signal without the nanoantenna [2]. The simplest way to evaluate the nanoantenna in term of its field enhancement *FE* is to measure the *contrast*, which is defined as the ratio of signal intensity measured with the nanoantenna and without it [3]:

$$Contrast = \frac{I_{near\,field}}{I_{far\,field}} = \frac{I_{with\,tip} - I_{without\,tip}}{I_{without\,tip}} = \\ = \frac{I_{with\,tip}}{I_{without\,tip}} - 1 \tag{1}$$

where $I_{near\,field}$ is defined as the Raman peak intensity due only to the interaction of the nanoantenna with the scattering material, which is the signal measured while the tip is interacting with the sample, $I_{with\,tip}$, subtracted by the signal when the tip is not interacting with the sample $I_{without\,tip}$. On the other hand, $I_{far\,field}$ is the intensity measured without the nanoantenna enhancement, which is equals to the intensity measured without the tip interacting with the sample, $I_{without\,tip}$.

While the contrast is sufficient to determine the FE in the case of an ideal zero-dimensional scatterer, such as a single molecule, in the case of a sample dispersed in a surface or volume, the amount of material contributing to the far-field and near-field signals have to be evaluated. The *FE* then is defined as the product of the contrast and the effective illumination area ratio between near- and far-field, namely the geometric factor *GF*, with

$$FE = contrast \times GF. \tag{2}$$

The GF evaluation depends on sample geometry, illumination pattern and tip properties. Considering a sample homogeneously distributed in a two-dimensional surface, we name $A_{focus} = \pi r_{focus}^2$ as the illumination area of the focused laser beam and $A_{tip} = \pi r_{tip}^2$ as the illumination area of the tip apex in the scattering surface. *GF* can then be evaluated as

$$GF = \frac{A_{focus}}{A_{tip}} = \frac{r_{focus}^2}{r_{tip}^2}. \tag{3}$$

Although largely accepted due to its simplicity [1], [4]–[9], this "back-to-the-envelop"-like theory is problematic. Different samples on different setups, and even different scattering

978-1-7281-2109-3/19/$31.00 © 2019 IEEE

TABLE I

FE VALUES AS A FUNCTION OF LASER SPOT RADIUS r_{focus} AND TIP RADIUS r_{tip} CALCULATED USING EQS. 2 AND 3 FOR A $contrast = 2.10$.

		Laser spot radius (nm)				
		160	**180**	**200**	**220**	**240**
Tip Radius (nm)	**15.0**	261	331	408	494	588
	17.5	192	243	300	363	432
	20.0	147	186	230	278	331
	22.5	116	147	181	219	261
	25	94	119	147	178	211

systems result in different contrast values for the same nanoantenna. Table I exemplifies how changes on r_{tip} and r_{focus} drastically vary the FE evaluation: Considering, without loss of generality, a measurement resulting in a $contrast$ of 2.1, using a tip of radius $(15 \pm 5)nm$ and laser focus radius of $(200 \pm 40)nm$, the resulting FE varies in values from *94* to *588* (see Table I).

Consequently, different authors may define the enhancement factor slightly differently, depending on the application [7]–[9]. Also, there is not an agreement in the TERS research community whether the FE is related to the experimental setup [1], [4], [10] or to the tip itself [5], [6]. In order to have TERS as an useful nanomaterials' characterization technique, it is urgent to minimize the arbitrariness in the definition of enhancement factor of a nanoantenna, providing a protocol to compare different nanoantennas in terms of their enhancement factor.

Here we define f_e as the intrinsic nanoantenna enhancement factor, and we propose a protocol and a reference material to measure f_e. This proposal consists of measuring the TERS intensity as a function of the tip-sample distance, named the tip-approach curve, in a reference standard material and fitting the experimental results using the theory derived in Ref. [11]. In the following sections we describe the methodology and compare the advantages in using the f_e obtained by this method in comparison to the result obtained with Eq. 2.

II. METHODOLOGY

The protocol proposed here is to measure f_e based in fitting the tip-approach curve $I_\Gamma^{TERS}(\Delta z)$, which depends on the tip-sample distance Δz. Figure 1 defines the relevant parameters. Considering the dipole located at the center of the sphere representing the tip apex, the total dipole-sample distance is given by $z = r_{tip} + z_0 + \Delta z$, where r_{tip} is the tip-apex sphere radius, and z_0 is the minimum distance achieved by the tip from the sample, as defined by the SPM setpoint. Γ and L_c are the phonon symmetry and coherence length, respectively.

A. Theory

Equation 4 expresses the Raman signal intensity $I_\Gamma^{TERS}(\Delta z)$ measured by a TERS system, as a function of the tip-displacement Δz, adapted from Ref. [11], for a phonon with symmetry Γ and coherence length L_c, and a tip with $FE = f_e$.

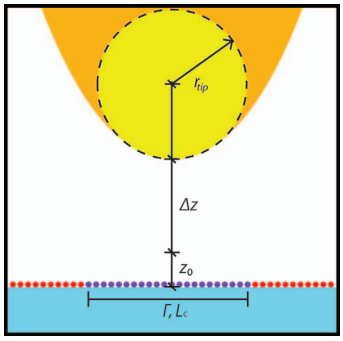

Fig. 1. Illustration of the relevant parameters for the definition of $I_\Gamma^{TERS}(\Delta z)$. The dipole excitation is located at the center of a sphere (yellow) with radius r_{tip}, at the apex of the nanoantenna (orange). The total dipole-sample distance is $z = z_0 + \Delta z + r_{tip}$, where Δz is the displacement from the initial setpoint z_0 in a tip-sample approach curve. The sample is represented by the small dots at the substrate surface. Given a phonon with symmetry Γ, the light field scattered by the region smaller then the phonon coherence length L_c (purple dots) exhibit interference. Outside this region (red dots), the vibrations in the material system are uncorrelated.

$$I_\Gamma^{TERS}(\Delta z) = C_\Gamma f_e^2 \left(\frac{f_e^2 r_{tip}^6}{z^8} g_\Gamma^{TST}(L_c, z) + g_\Gamma^{ST}(L_c, z) \right) \tag{4}$$

The complete algebraic form of Eq. 4 can be found in Ref. [11]. Here we just want to specify that I_Γ^{TERS} has two contributions: The functions g^{TST} and g^{ST} related to the scattering modes *TST* and *ST*, which accounts for the sample-tip-sample and the sample-tip interactions, respectively [11], [12].

In addition to the scattering modes, the $I_\Gamma^{TERS}(\Delta z)$ depends on sample, tip and instrumental aspects. The sample aspects are the vibrational mode phonon symmetry Γ and the phonon coherence length L_c. The tip aspects are the r_{tip} and the f_e. The instrumental aspects are z_0 and the constant C_Γ. Although C_Γ accounts for the Raman cross section of the Γ symmetry mode (an intrinsic sample property), it is highly dependent on instrumental factors, such as detectors sensitivity, laser intensity and system alignment. In order to get a better understanding of Eq. 4 and how to use it in a protocol to determine f_e, it is important to understand how Γ, L_c, r_{tip} and f_e influence the tip-approach curve.

For studying the Γ and L_c influences in $I_\Gamma^{TERS}(\Delta z)$, consider the fixed the parameters $f_e = 5$, $r_{tip} = 15nm$ and $z_0 = 3nm$ (see Table II). Figs. 2a,b show the graphs for different symmetry modes mixing the A_{1g} and E_{2g} symmetries for a fixed value of $L_c = 30nm$. These symmetries were chosen to simulate the results from graphene, where the Raman peaks *G* and *G'* bands are related to the E_{2g} and A_{1g} symmetry modes, respectively [13]. Fig. 2a shows the absolute $I_\Gamma^{TERS}(\Delta z)$ in a log-log plot for $C_\Gamma = 1$. In Fig. 2b the same result is displayed but normalized at $\Delta z = 0$.

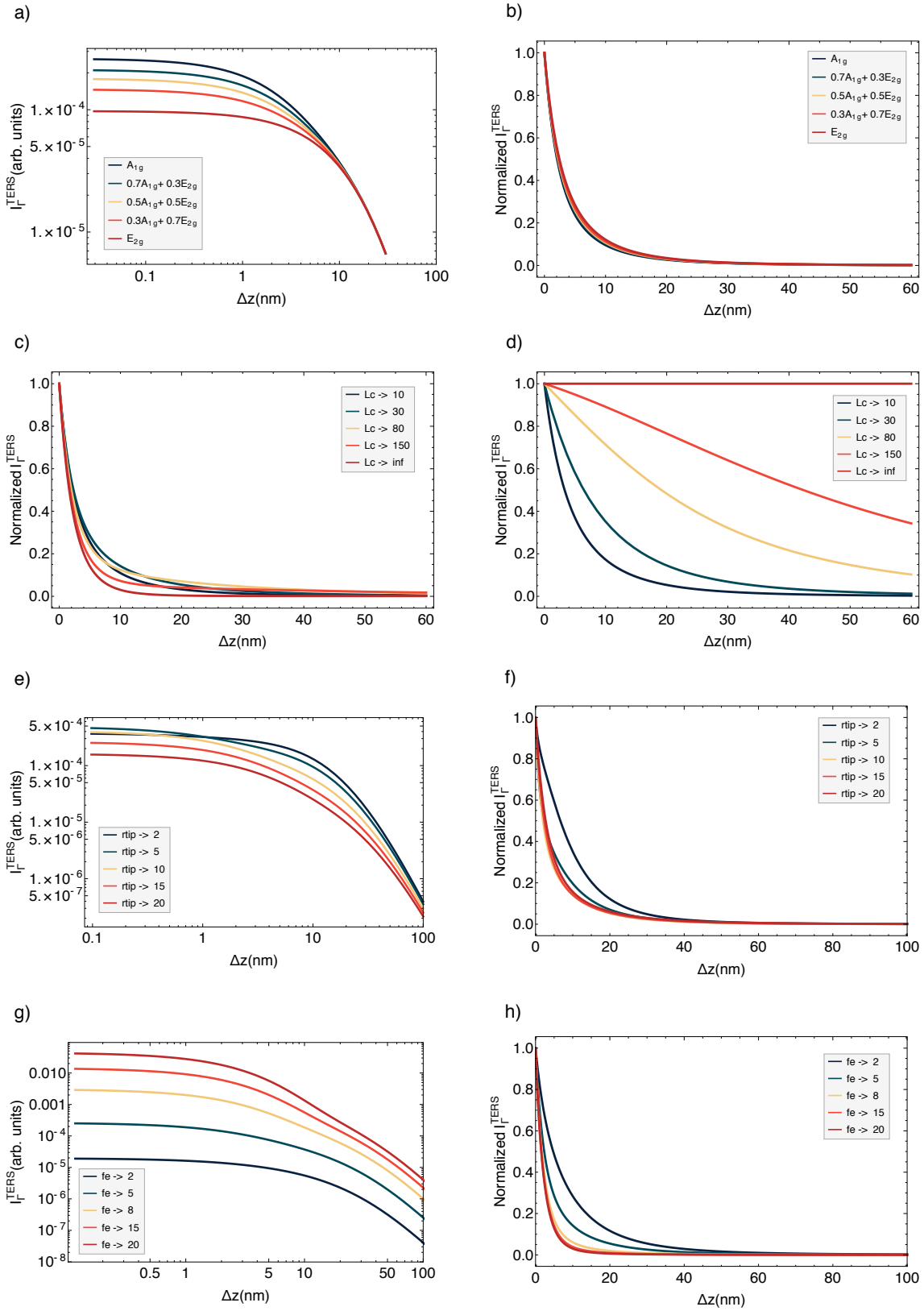

Fig. 2. All graphics represent the tip-approach curves - $I_{\Gamma}^{TERS}(\Delta z)$ as a function of tip-displacement Δz. In each graph, one parameter is variable and all other parameters fixed, as summarized in Table II. (a, e, g) are log-log plots, while the others exhibit a linear scale and are normalized. The normalization process consists in dividing each curve by its value at $\Delta z = 0$.

TABLE II
PARAMETERS USED TO PLOT THE GRAPHICS IN FIG.02

Panel	Scale	Fixed parameters	emphasized parameter
a)	Log-log	f_e = 5 r_{tip} = 15 nm z_0 = 3 nm L_c = 30 nm	phonon symmetry Γ
b)	Linear	f_e = 5 r_{tip} = 15 nm z_0 = 3 nm L_c = 30 nm	phonon symmetry Γ
c)	Linear	f_e = 5 r_{tip} = 15 nm z_0 = 3 nm $\Gamma = A_{1g}$	phonon coherence length L_c
d)	Linear	f_e = 5 r_{tip} = 15 nm z_0 = 3 nm $\Gamma = E_{2g}$	phonon coherence length L_c
e)	Log-log	f_e = 5 z_0 = 3 nm L_c = 30 nm $\Gamma = A_{1g}$	tip apex radius r_{tip}
f)	Linear	f_e = 5 z_0 = 3 nm L_c = 30 nm $\Gamma = A_{1g}$	tip apex radius r_{tip}
g)	Log-log	r_{tip} = 15 nm z_0 = 3 nm L_c = 30 nm $\Gamma = A_{1g}$	enhancement factor f_e
h)	Linear	r_{tip} = 15 nm z_0 = 3 nm L_c = 30 nm $\Gamma = A_{1g}$	enhancement factor f_e

In the normalized picture, the faster the decay of the intensity as Δz increases, the larger the effective enhancement. The A_{1g} mode exhibits the larger enhancement, in agreement with [11], [13], [14].

Now, fixing the symmetry mode and varying the L_c, using the same tip parameters as in Fig. 2a,b, Figs.2c and 2d show the tip-approach curves for the A_{1g} and E_{2g} symmetry modes, respectively (parameters summarized in Table II). For the A_{1g} mode (G band), Fig. 2c, from $L_c \to 0$ to $L_c = 80nm$, indicated by the dark-blue line and yellow lines, respectively, the dependence with Δz are smother, showing that the *ST* scattering mode plays a more important role in these scattering events. By increasing the L_c value further, represented by the orange and red lines, the curves changes their behavior with Δz, decaying faster for smaller values of Δz , showing that the *TST* mode is more relevant after L_c values between 30 and 80nm, tending to the red curve for $L_c \to \infty$.

Fig. 2d shows the same plot for the E_{2g} mode. Again, the slope of the curves indicates that the ST scattering gets more relevant for larger values of L_c. For $L_c \to \infty$, the curve approaches to a constant value, indicating no tip-induced enhancement for the fully coherent E_{2g} scattering due to destructive interference, in agreement with [11], [13], [14].

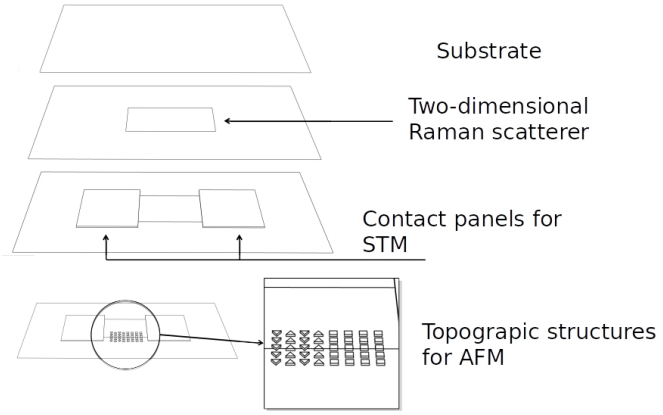

Fig. 3. Schematics illustrates the TERS calibration device. From top to bottom: 1) Transparent substrate; 2) Pristine monolayer graphene; 3) Contact panels made with conducting material for STM; 4) Topographic structures with different geometries for AFM calibration with well-defined edges.

B. Fitting the Tip-approach Curves

The theory described in this section can now be used in a protocol to estimate f_e, as evidenced by the results displayed in Fig. 2. It is crucial to have the z_0 and r_{tip} values well established and the sample properties L_c and Γ well defined. For this reason, it is important to have a reference material. To avoid the instrumental aspects hidden in C_Γ, it is also important to work with the normalized data. After a normalized tip-approach curve data is extracted from such a reference material, the protocol includes adjusting the data by choosing the value of f_e that better describes the normalized $I_\Gamma^{TERS}(\Delta z)$ curve. A graphene device is proposed here for the reference material because graphene is a widely studied 2D material [15] with a well-defined L_c [14].

C. Reference Material

A few parameters have to be calibrated in a TERS system in order to be able to obtain the best performance of a nanoantenna. These parameters influence on the accuracy of the Raman spectral frequencies, spectral imaging and scanning probe imaging. The proposed reference material consists of a device that helps on these calibrations (see Fig. 3). The same platform can then be used to obtain f_e and, subsequently, to perform repeatable or traceable TERS experiments *in situ*. The components of the reference materials are described in Fig. 3, which comprises:

- **Substrate**: The substrate have to be a material with no optical response in the same range of a graphene Raman scatter. Glass, fused quartz or other transparent media are ideal for sample illumination from the bottom.
- **Two-dimensional Raman scatterer**: graphene for confocal and TERS calibration.
- **Contact panels for STM**: in the case SPM is utilized in the STM mode, for current drain.
- **Topographic arrangement for AFM**: periodic topographic structure with well-defined dimensions for calibration of the SPM system in the AFM mode.

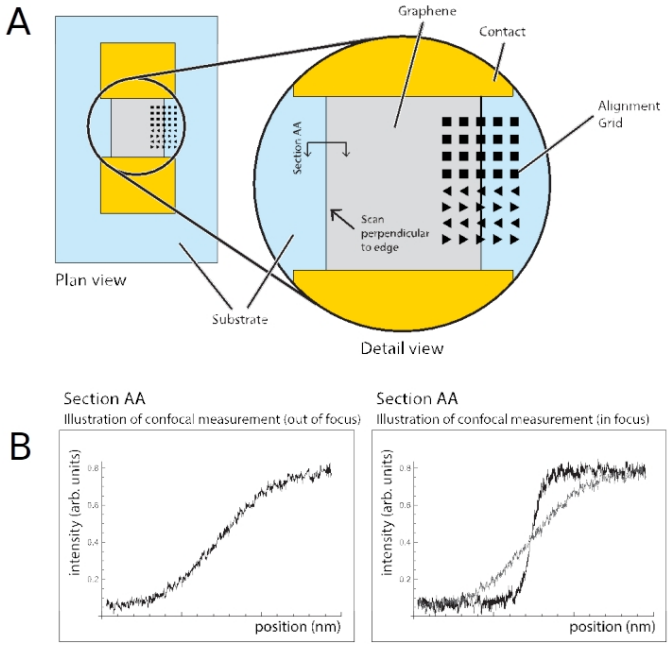

Fig. 4. A schematics of the calibration device. The detailed view of A illustrates how the lateral scan must be performed to maximize the SNOM lateral resolution. B illustrates a misaligned system before calibration (left) and the expected signal after alignment in comparison with the first (right).

D. Experimental Protocol

1) Alignment of Scanning Confocal Optical Microscope: The scanning confocal optical microscope (SCOM) is the first system to be aligned and, in order to do that, it is ideal to have a sample that provides a strong Raman signal, with well-defined topological edges. This alignment is performed by moving the laser beam in and out of the material to maximize the optical lateral (X/Y) resolution (Fig. 4).

The proposed platform provides a single layer graphene for the alignment of the SCOM system. Graphene is considered an ideal material for this step, due to its strong Raman signal and its truly bidimensional structure. By scanning in and out of the graphene sheet, the user is able to maximize the lateral resolution. This can be directly observed through the slope of the signal generated when the laser moves in and out of the graphene sheet. The steeper the slope, the better the optical lateral resolution of the system (Fig. 4B). The expected resolution for a good, well-aligned optical system is approximately half the wavelength of the excitation laser being used.

2) Configuration of Scanning Probe Optical Microscope: With the SCOM aligned, the second step is to configure the scanning optical microscopy (SPOM) system. The requirement in this step is to align the tip apex with the laser focal point. The proposed platform provides a topographic alignment grid designed not only to facilitate this task (see Fig. 5), but also to allow a quick and effective in-situ inspection of the tip apex radius .

To provide meaningful information for tip alignment, the grid has both square and triangular shapes. By using the triangular shapes as reference for alignment, it is possible to have relative tip-focus position information along both X and Y directions while scanning only in one direction (Fig. 5). By scanning over the topographic grid and comparing the generated confocal and topographical images, the user can see how misaligned the tip is with respect to the focal point, and to adjust the tip position in real time. The geometrical nature of the topographic grid facilitates the alignment procedure, by providing the user an easy way to calculate the tip to focus offset direction and distance.

In addition, this procedure can be used to evaluate the r_{tip}. This parameter is crucial to minimize the error in estimating the f_e by fitting the tip-approach curve.

3) Tip-approach: After the alignment of both SCOM and SPOM using this protocol, and having the r_{tip} characterized by the tip lateral resolution, the next step is finally the determination of f_e for a given phonon mode Γ.

The tip-approach curve consists in measuring the Raman Intensity $I_\Gamma^{TERS}(\Delta z)$ for different Δz values in the same XY position of the reference standard material (on top of graphene).

The absolute I_Γ^{TERS} values depends on the defined C_Γ, which includes environment aspects, such as distance to the detector. To eliminate this factor from our analysis, the signal should be normalized. All points must be divided by the Raman intensity obtained at $\Delta z = 0$. The f_e value is the one that better adjusts the tip-approach curves.

III. Conclusion

This protocol and reference material were developed in order to have an approach to differentiate the intrinsic nanoantenna enhancement factor f_e. As detailed in Section II, the protocol is based on the fitting of a tip-approach curve, the $I_\Gamma^{TERS}(\Delta z)$, with Eq. 4.

The parameters influencing the tip-approach curve shape were presented in the Subsection II-A and summarized in Fig 2. Both sample proprieties, Γ and L_c, and tip properties r_{tip} and f_e, influence in the behavior of the tip-approach curve. In order to measure the f_e, the parameters Γ, L_c and r_{tip}, must be measured. Therefore, the reference material described in II-C is a graphene-based device with well-defined Γ and L_c, to check r_{tip} and check the whole alignment of the system, by following the experimental protocol described in II-C.

With this article, authors expectation is to minimize the arbitrariness of the definition of f_e for a TERS nanoantenna, and to provide an useful guide to measure it, providing a value to compare nanoantennas by means of their enhancements.

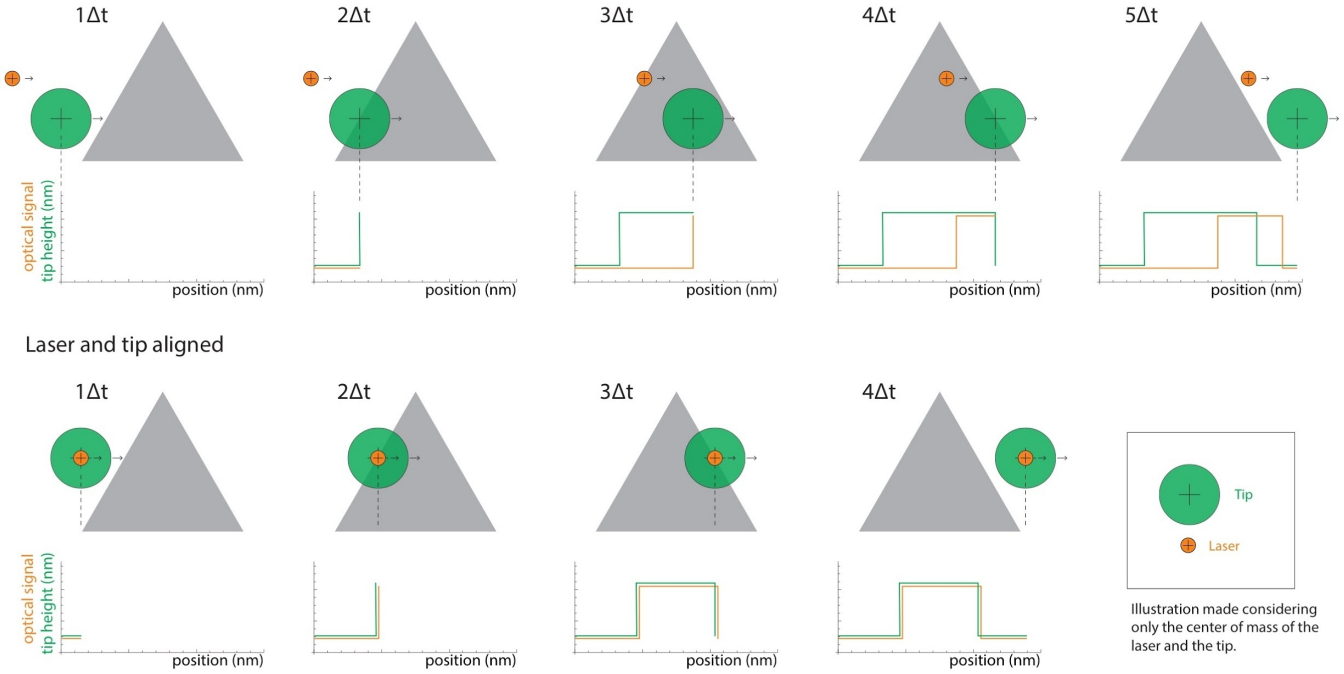

Fig. 5. This figure illustrates the scanning of topographic structure (gray triangle), considering (top) the situation when the tip SPM (orange circle) is misaligned with the laser spot (green circle), and (bottom) the situation when the tip and optical signal are aligned. The expected measured line profiles are bellow the figures. For the AFM tip, it is a measured of the tip height as a function of the lateral position. For the optics, it represents the measured signal intensity as function of the lateral position. By measuring both optical signal and tip-height as a function of the lateral movement, it is possible to infer whether the tip is aligned with the optical signal in the XY plane.

REFERENCES

[1] J. Stadler, T. Schmid, and R. Zenobi, "Developments in and practical guidelines for tip-enhanced Raman spectroscopy," *Nanoscale*, vol. 4, no. 6, pp. 1856–1870, 2012.

[2] P. Verma, "Tip-Enhanced Raman Spectroscopy: Technique and Recent Advances," *Chemical Reviews*, vol. 117, no. 9, pp. 6447–6466, 2017.

[3] B. Pettinger, P. Schambach, C. J. Villagómez, and N. Scott, "Tip-Enhanced Raman Spectroscopy: Near-Fields Acting on a Few Molecules," *Annual Review of Physical Chemistry*, vol. 63, no. 1, pp. 379–399, 2012.

[4] S. Kawata, *Tip enhancement*. Amsterdam Oxford: Elsevier, 2007.

[5] N. Kumar, A. Rae, and D. Roy, "Accurate measurement of enhancement factor in tip-enhanced Raman spectroscopy through elimination of far-field artefacts," *Applied Physics Letters*, vol. 104, no. 12, 2014.

[6] M. Nicklaus, *Tip-Enhanced Raman Spectroscopy for Nanoelectronics*. Norderstedt: Books on Demand, 2014.

[7] D. Mehtani, N. Lee, R. D. Hartschuh, A. Kisliuk, M. D. Foster, A. P. Sokolov, F. Čajko, and I. Tsukerman, "Optical properties and enhancement factors of the tips for apertureless near-field optics," *Journal of Optics A: Pure and Applied Optics*, vol. 8, no. 4, pp. S183–S190, 2006.

[8] D. S. Bulgarevich and M. Futamata, "Apertureless Tip-Enhanced Raman Microscopy with Confocal Epi-Illumination / Collection Optics," *Applied Spectroscopy*, vol. 58, no. 7, pp. 757–761, 2004.

[9] N. Jiang, E. T. Foley, J. M. Klingsporn, M. D. Sonntag, N. A. Valley, J. A. Dieringer, T. Seideman, G. C. Schatz, M. C. Hersam, and R. P. Van Duyne, "Observation of multiple vibrational modes in ultrahigh vacuum tip-enhanced Raman spectroscopy combined with molecular-resolution scanning tunneling microscopy," *Nano Letters*, vol. 12, no. 10, pp. 5061–5067, 2012.

[10] L. Meng, T. Huang, X. Wang, S. Chen, Z. Yang, and B. Ren, "Gold-coated AFM tips for tip-enhanced Raman spectroscopy: theoretical calculation and experimental demonstration," *Optics Express*, vol. 23, no. 11, p. 13804, 2015.

[11] L. G. Cançado, R. Beams, A. Jorio, and L. Novotny, "Theory of spatial coherence in near-field Raman scattering," *Physical Review X*, vol. 4, no. 3, pp. 1–14, 2014.

[12] L. Novotny and B. Hecht, *Principles of Nano-Optics*. Cambridge University Press, 2012.

[13] A. Jorio, N. S. Mueller, and S. Reich, "Symmetry-derived selection rules for plasmon-enhanced Raman scattering," *Physical Review B*, vol. 95, no. 15, pp. 1–10, 2017.

[14] R. Beams, L. G. Cançado, S. H. Oh, A. Jorio, and L. Novotny, "Spatial coherence in near-field Raman scattering," *Physical Review Letters*, vol. 113, no. 18, pp. 1–5, 2014.

[15] A. Jorio, "Raman Spectroscopy in Graphene-Based Systems: Prototypes for Nanoscience and Nanometrology," *ISRN Nanotechnology*, vol. 2012, no. 2, pp. 1–16, 2012.